Adaptive Generalized Predictive Controller and Cartesian Force Control for Robot Arm Using Dynamics and Geometric Identification

Shohei Hagane, Liz Katherine Rincon Ardila, Takuma Katsumata, Vincent V. Bonnet, Philippe Fraisse, Gentiane Venture

https://doi.org/10.20965/jrm.2018.p0927

Paper:

Adaptive Generalized Predictive Controller and Cartesian Force Control for Robot Arm Using Dynamics and Geometric Identification

Shohei Hagane[*1], Liz Katherine Rincon Ardila[*1], Takuma Katsumata[*2], Vincent Bonnet[*3], Philippe Fraisse[*4], and Gentiane Venture[*1]

[*1]Tokyo University of Agriculture and Technology
2-24-16 Nakacho, Koganei City, Tokyo 184-8588, Japan
E-mail: gvinfo@cc.tuat.ac.jp
[*2]Yahoo Japan Corporation
Kioi Tower, Tokyo Garden Terrace Kioicho, 1-3 Kioicho, Chiyoda-ku, Tokyo 102-8282, Japan
[*3]Electrical Engineering and Robotics, University of Paris-Est Créteil
61 Avenue Général de Gaulle, 94000 Créteil, France
[*4]Université de Montpellier
LIRMM, 161 Rue ADA, 34095 Montpellier, France
[Received February 26, 2018; accepted October 3, 2018]

In realistic situations such as human-robot interactions or contact tasks, robots must have the capacity to adapt accordingly to their environment, other processes and systems. Adaptive model based controllers, that requires accurate dynamic and geometric robot's information, can be used. Accurate estimations of the inertial and geometric parameters of the robot and end-effector are essential for the controller to demonstrate a high performance. However, the identification of these parameters can be time-consuming and complex. Thus, in this paper, a framework based on an adaptive predictive control scheme and a fast dynamic and geometric identification process is proposed. This approach was demonstrated using a KUKA lightweight robot (LWR) in the performance of a force-controlled wall-painting task. In this study, the performances of a generalized predictive control (GPC), adaptive proportional derivative gravity compensation, and adaptive GPC (AGPC) were compared. The results revealed that predictive controllers are more suitable than adaptive PD controllers with gravitational compensation, owing to the use of well-identified geometric and inertial parameters.

Keywords: adaptive optimal control, generalized predictive control (GPC), simulation, robot arm, KUKA LWR

1. Introduction

Robotic serial manipulators are widely used in various industrial fields [1, 2]. Due to their accuracy and repeatability, they can manufacture increasingly complex products in a shorter production time. Industrial manipulators are typically position-driven by commonly known proportional-integral-derivative (PID) controllers, and the parameters are tuned based on a fixed robot model. In the case of human-robot interactions (co-botics) [3, 4], force control is required to address environmental uncertainties [5]. A force controller is typically based on force sensors, which are expensive, fragile, and require frequent calibrations. Alternatively, external forces can be estimated besides using force sensors, by using accurate dynamic and kinematic models of the robotic arm. With joint position sensors and torque sensors, which are already installed in the robot, force control can be performed by exploiting robot's dynamic and kinematic models and estimating external forces [6, a].

The estimation of external forces has been the focus of several studies conducted by the scientific community [7, 8]. Joint torque measurements and model-based disturbance observers are typically used for the estimation. Moreover, external forces are estimated as deviations from the model prediction [7, 9–11]. Therefore, the accuracy of the estimation depends on the accuracy of the segment lengths and segment inertial parameters (SIPs), which are required for the development of the kinematic and dynamic models. Generally, the robot controllers are based on parameters obtained from the computer-aided design (CAD) data. However, the CAD data does not include information on several internal robot components, and it is typically subject to delayed updates. Moreover, the CAD data is typically fixed; thus modifications made to the end-effector in the case of a multi-purpose manipulator are not considered. The focus of several studies has been the identification of the serial manipulator SIP [12–16]. The least-square and maximum likelihood estimation methods are the most popular approaches. Furthermore, the accuracy of SIP estimation is related to the maximization of information, i.e., the design of optimal exciting trajectories [17–20].

Robotic arms are capable of using various types of tools. However, the dynamic characteristics of the robot vary when a tool is being held by the robot, especially when the mass of the tool is relatively high. The additional mass and length at the end-effector may result in an inaccurate control performance if the robot is only operated using position control and a conventional PID controller. Thus, in this study, an adaptive predictive position-force control framework that uses geometric and dynamic identification was proposed. This method can be used for any serial manipulator equipped with joint torque sensors or equivalent sensors (for motor-current measurement); enabling the manipulator to accurately perform various tasks using different tools, without loss of performance.

To achieve better control performances, the adaptive predictive controller using generalized predictive control (GPC) was proposed. The model parameters used in the GPC were based on the results of a fast dynamic and geometric identification process. GPC is a controller in the model predictive controls (MPC) category [21,22]. It was developed by Clarke [23], and it is now widely used in industry and academia [24–26]. Moreover, it was successfully implemented in several industrial applications with good performance and adequate robustness [21, 24, 27]. M. Makarov et al. [28] applied GPC to an anthropomorphic robotic arm, and it demonstrated a superior tracking and robustness to that of PID controllers. Furthermore, GPC can handle several control problems [29] for a wide range of plants with a significant number of design variables, which have to be specified by the user based on prior knowledge of the plant and control objectives. By coupling it with identification, reliable inertial parameters of the robotic arm can be obtained, and a high-quality GPC can be designed using the inertial information. A feedback linearization technique was used to apply the GPC method to the robotic arm. However, the quality of feedback linearization depends on the accuracy of the dynamics model of the robot and the feedback information such as the angular acceleration, which is difficult to obtain on time in real-time.

Other adaptive controllers that use predictive laws such as the extended horizon adaptive control (EHAC) proposed by B. E. Ydstie, or the extended prediction self-adaptive control (EPSAC) proposed by Keyser and Van Cauwenberghe were developed [30–33]. In the EHAC control, the adaptation of the control law depends on the system parameters. The controller adapts the final prediction horizon and fixes the optimal weighting parameter (λ). The parameters are updated over a long period of time in the process, and the coefficients of the prediction equation cannot be obtained at certain points in time. Moreover, the controller produces a reduced functionality to calculate the control effort, and an extension of the horizon results in a delayed velocity response [30]. The EPSAC updates the prediction horizon, weighting factor, and filter polynomials. However, the on-line adaptation affects the structure of the predictor and control, which may lead to unstable motions.

In this study, a novel control adaptation scheme based on the adaptive generalized predictive control (AGPC) using the robot dynamic and geometrical identification with optimal exciting motions was designed. The adaptation can calculate the optimal weighting function λ, and directly modify the optimal predictor in the cost function, which updates the law of control. The scheme adapts the parameters of the reference dynamics model using the on-line dynamic and geometric information of the robot, and it optimizes the system to obtain the new predictor. The optimal predictor is calculated to ensure stability over the full range of robotic motion. The adaptive position and force controllers were designed and evaluated for the KUKA robotic arm. Although a wall painting task using different types of painting rollers is presented in this paper, the system can perform other tasks that involve the grasping or manipulation of objects. In these cases, the accuracy of the position control is more crucial for the completion of the task.

2. Paper Contributions

In the context of this study, novel methods for adaptive controllers using the predictive laws based on the fast robot dynamic and geometric identification with optimal exciting motion were proposed. Moreover, the contributions of this study are as follows:

I) The development of the predictive controllers with a proposal of a new scheme of adaptation and predictive actions based on the fast dynamic and geometric identification with optimal trajectories.

II) The estimation of control parameters for the optimal predictor, with respect to the dynamic and geometric modeling of the robot.

III) The adaptive generalized predictive control using exciting optimal motion trajectories with constrained optimization.

IV) The application of a method for the estimation of the external forces (without force sensors) based on the dynamic identification results, to generate the adaptation of the predictive motion in the control system.

An overview of the framework proposed in this paper is presented in **Fig. 1**. In this study, the framework was applied to the KUKA lightweight robot (LWR) and it was generalized for any robotic arm platform. In Section 3, the geometric and dynamic models of the KUKA LWR are described. Section 4 presents the parameter identification of the robot using optimal exciting trajectories. In Section 5, the reference motion planning is discussed. Section 6 presents the development of the robot control system with position and force controls, and the application of the adaptation with the novel prediction scheme. In Section 7, the experimental setup is presented; followed by the results and discussion in Section 8.

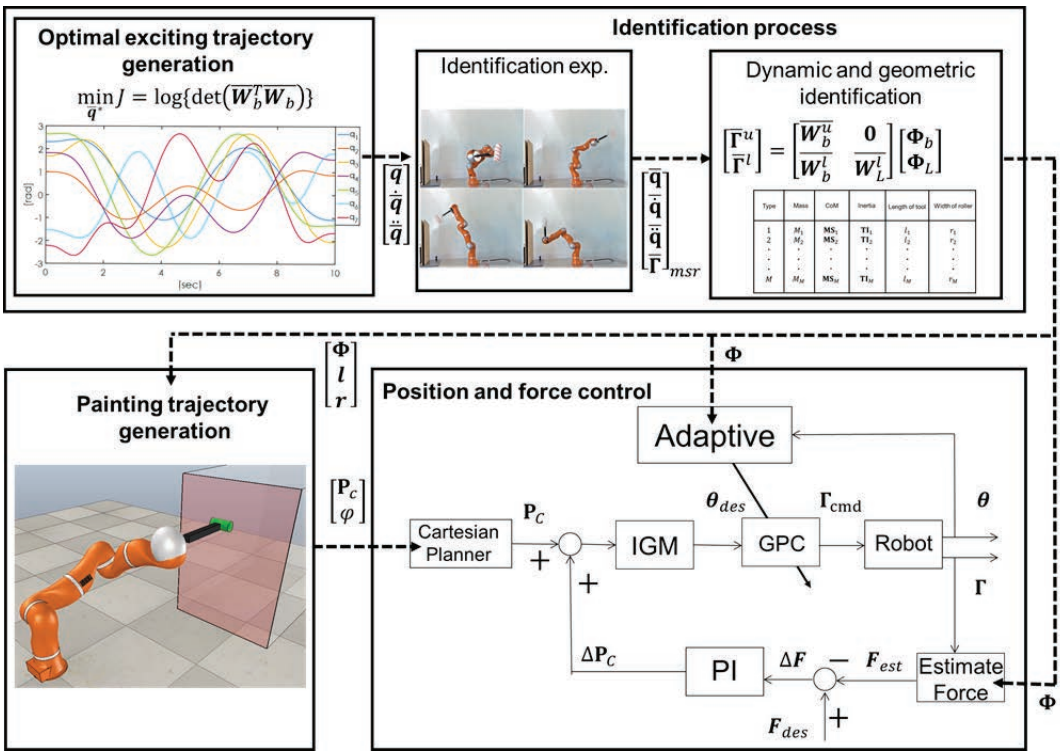

Fig. 1. Overview of the proposed framework for adaptive predictive controllers based on dynamic and geometric identification with optimal exciting motion.

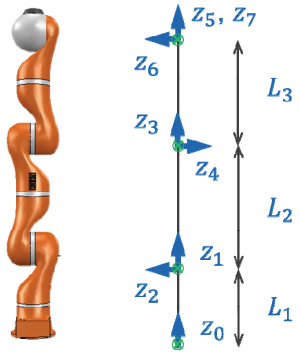

Fig. 2. Frames and segments definitions for the KUKA LWR used in the MDH in **Table 1** [34].

Table 1. Modified DH parameters of the KUKA LWR.

i	a_i	μ_i	σ_i	α_i	d_i	θ_i	r_i
1	0	1	0	0	0	θ_1	L_1
2	1	1	0	$\pi/2$	0	θ_2	0
3	2	1	0	$-\pi/2$	0	θ_3	L_2
4	3	1	0	$-\pi/2$	0	θ_4	0
5	4	1	0	$\pi/2$	0	θ_5	L_3
6	5	1	0	$\pi/2$	0	θ_6	0
7	6	1	0	$-\pi/2$	0	θ_7	0

3. Modeling of KLWR

3.1. Geometric Model

The KUKA LWR (KLWR) is a manipulator with a kinematic redundancy similar to that of the human arm, i.e., with seven degrees of freedom (DoFs) (**Fig. 2**). The KLWR has a load-to-weight ratio of approximately 1 : 1, whereas industrial robots typically have a ratio of 1 : 10 or lower [4]. The total mass of the arm is approximately 17 kg with a 1.2 m work space. Each link has an angle and torque sensor, and in this case, the position control and torque control could be easily performed. Using the modified Denavit-Hartenberg (MDH) parameters (**Table 1**), the forward kinematics model was calculated. The segment lengths L_1, L_2, L_3 were set using the available CAD data [12, b].

In this study, the controllers for the KLWR were managed from the robot task space. Therefore, an inverse geometric model of the KLWR was required. The inverse geometric model is generally calculated using the Paul method. However, given that the KLWR has seven DoFs, the calculation of its inverse geometric model was not trivial. To solve the redundancy problem in the robot, a swivel angle φ was added to the model [35], and the Paul method was then implemented to obtain the resolution of the inverse geometric model. With this approach, the elbow was free to move along a circular arc with a normal vector parallel to the axis defined from the shoulder to the wrist, for any given end-effector pose.

In **Fig. 3**, $\mathbf{P}_s, \mathbf{P}_e, \mathbf{P}_w$ define the position of the shoulder,

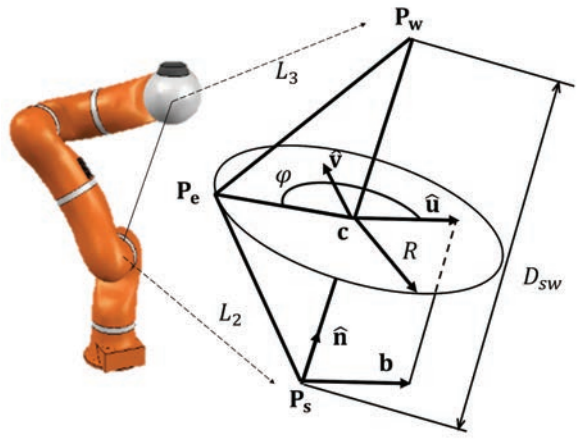

Fig. 3. For any pose of the robot end-effector, the elbow joint moves freely in a circular trajectory of swivel angle φ.

elbow, and wrist of the robot, respectively. The swivel angle φ uniquely defines the position of the elbow $\mathbf{P}_e$ on a circular trajectory, which is orthogonal to vectors $[(\mathbf{P}_s\mathbf{P}_w)]$. To mathematically describe this circle, the unit vector $\hat{\mathbf{n}}$ of the direction from the shoulder to the wrist was defined. A local coordinate system was created from unit vectors $\hat{\mathbf{u}}$ and $\hat{\mathbf{v}}$. It can be noted that $\hat{\mathbf{u}}$ was arbitrarily set to be the projection of a user-defined vector $\mathbf{b}$. The mathematical description of $\hat{\mathbf{u}}$, $\hat{\mathbf{v}}$, and $\hat{\mathbf{n}}$ is found in [35].

3.2. Dynamic Model

The inverse dynamic model of the KLWR was calculated using Newton-Euler equations, to obtain the joint torques vector $\mathbf{\Gamma}$ [36]:

$$\begin{cases} \mathbf{\Gamma} = \mathbf{M}(\mathbf{q})\ddot{\mathbf{q}} + \mathbf{C}(\mathbf{q},\dot{\mathbf{q}}) + \mathbf{G}(\mathbf{q}) + \mathbf{\Gamma}_f + \mathbf{\Gamma}_{ext} \\ \mathbf{\Gamma}_f = \mathrm{diag}(\dot{\mathbf{q}})\mathbf{FV} + \mathrm{diag}(\mathrm{sign}(\dot{\mathbf{q}}))\mathbf{FC} \end{cases} \quad (1)$$

where $\mathbf{q}$, $\dot{\mathbf{q}}$, and $\ddot{\mathbf{q}}$ represents the (7×1) vectors of the joint angles, velocities, and accelerations; $\mathbf{M}(\mathbf{q})$ (7×7) represents the robot tensor of the inertia; $\mathbf{C}(\mathbf{q},\dot{\mathbf{q}})$ (7×1) represents the Coriolis and centrifugal terms; and $\mathbf{G}(\mathbf{q})$ (7×1) is the gravitational term. Moreover, $\mathbf{\Gamma}_{ext}$ is the joint torques vector, which represents the influence of the external forces; and $\mathbf{\Gamma}_f$ (7×1) is the vector of the friction torques due to Coulomb and viscous-friction effects. Furthermore, $\mathbf{FC} = [FC_1 \cdots FC_{NJ}]^T$ (7×1) is the vector containing the Coulomb's friction coefficients, and $\mathbf{FV} = [FV_1 \cdots FV_{NJ}]^T$ (7×1) is the vector containing the viscous friction coefficients.

The equations of motion can be expressed in linear form with respect to the inertial parameters in the joint frames [13] as follows:

$$\mathbf{W}(\mathbf{q},\dot{\mathbf{q}},\ddot{\mathbf{q}})\mathbf{\Phi} = \mathbf{\Gamma} \quad . \quad . \quad . \quad . \quad . \quad . \quad . \quad . \quad . \quad . \quad . \quad . \quad (2)$$

where $\mathbf{W}$ (7×84) is the regressor of the chains, $\mathbf{\Phi}$ (84×1) is the vector of standard inertial parameters to be identified, and $\mathbf{\Phi} = [\mathbf{\Phi}_1^T \quad \mathbf{\Phi}_{NL}^T \quad \mathbf{FC}^T \quad \mathbf{FV}^T]^T$.

For each segment i, 10 inertial parameters can be expressed in the joint frame $\mathbf{\Phi}_i = [M_i \quad \mathbf{MS}_i^T \quad \mathbf{TI}_i^T]^T$, where M_i is the mass, $\mathbf{MS}_i = [MSX_i \quad MSY_i \quad MSZ_i]^T$ is the three-dimensional vector of the first moment of inertia, and the six-dimensional vector $\mathbf{TI}_i = [XX_i \quad YY_i \quad ZZ_i \quad XY_i \quad XZ_i \quad YZ_i]^T$ that gathers the components of the 3×3 tensor of inertia.

4. Identification of Robot Parameters

Adaptive controllers are based on the dynamic and geometric models of the robot. To precisely estimate each parameter, the identification method using the optimal exciting motion for fast robot identification described in [34] was implemented. The complete identification can be divided into three stages: i) the generation of the optimal exciting motions, ii) the identification of the robot inertial parameters, and iii) the end-effector tool identification (dynamic and geometric identification).

The robot identification and control system procedure were developed on two levels. The first level involved the identification of the dynamic parameters of the robot and painting rollers, to create the complete dynamic and kinematic models of the robot, including the painting rollers attached to the end-effector. The identification was conducted with fully exciting optimal trajectories to detect all the parameters of the robot and rollers with minimum errors and deviations. The optimal exciting trajectories were based on B-spline trajectory parametrization and the *log determinant* exciting criterion. The definition of the optimization problem includes the physical limitations of the joint angles, velocity, acceleration, and maximal torque. Furthermore, the optimal exciting trajectories include constraints to prevent auto-collision and collisions with the environment. The results of this full identification were applied to the base of the models and the system design of the control.

The second level involves the development of the painting task with controllers that were based on the results of the previous identification, to update the models in real-time. Moreover, they were used in the control design, which is discussed in Section 6. In this work, PD + Grv, GPC + feedback linearization, and AGPC were investigated. Each controller utilizes the identified dynamic parameters of the robot and rollers. In particular, GPC and AGPC are based on the dynamic models, and updating the parameters of the robot is a crucial task for the controllers if the characteristics of the robot varies with different types of rollers attached to its end-effector. Accurate parameters can be obtained after a change from the previous set using minimal information, given that only small variations require detection. In Section 6, the proposed AGPC that exploits the identified results of level one is presented. This adaptation was implemented during the execution of the painting task on-line. Given that the robot is a non-linear variant system, the values of the inertia matrix elements varied during the motion. The AGPC updates the inertia matrix using the identified information (level one). Moreover, the AGPC adapts its design param-

eters during the painting task.

The identification of the base parameters was developed by using the solution of Eq. (3) to determine the $\mathbf{\Phi}$ vector that contains the standard inertial parameters (SIP). Rewriting this equation with respect to the base parameters (BPs) as expressed by [14]; the vector $\mathbf{\Phi}_b$ $(N_b \times 1)$, which is the minimal set of inertial parameters required to define the robot dynamics, can be solved. The BPs are related to the kinematic structure of the robot, and they can be numerically computed [15].

$$\mathbf{W\Phi} = \mathbf{W}_b\mathbf{\Phi}_b = \mathbf{\Gamma} \quad . \quad . \quad . \quad . \quad . \quad . \quad . \quad . \quad . \quad . \quad . \quad . \quad (3)$$

The end-effector tool used by the robotic arm can be changed and modified. Moreover, it generates geometric and dynamic changes in the system. The geometric parameters of the end-effector tool were identified using its SIP, as described in [16, 34].

The dynamic identification of the end-effector was developed using a specific identification model based on two sets of grouped equations that represent the trajectories without and with the end-effector [37] by

$$\begin{bmatrix} \overline{\mathbf{\Gamma}}^u \\ \overline{\mathbf{\Gamma}}^l \end{bmatrix} = \begin{bmatrix} \overline{\mathbf{W}}_b^u & 0 \\ \overline{\mathbf{W}}_b^l & \overline{\mathbf{W}}_L^l \end{bmatrix} \begin{bmatrix} \mathbf{\Phi}_b \\ \mathbf{\Phi}_L \end{bmatrix} \quad . \quad . \quad . \quad . \quad . \quad . \quad . \quad (4)$$

where the upper and lower equations represent the trajectories without and with the end-effector, respectively. Moreover, $\overline{\mathbf{\Gamma}}^u$, $\overline{\mathbf{\Gamma}}^l$, $\overline{\mathbf{W}}_b^u$, $\overline{\mathbf{W}}_b^l$ represent the measured joint torques vectors and BP regressor matrices that correspond to the end-effector inertial parameters when the KLWR is unloaded and loaded, respectively.

The end-effector geometric identification is based on the relationship between the inertial and geometric parameters [38]. Moreover, the length and width of a paint roller can be determined from the look-up table. This table contains the inertial and geometric parameters for each painting tool. A principal component analysis (PCA) of the inertial parameters [39] is conducted for the classification and discrimination of the different tool characteristics.

Several studies have been conducted to generate optimal exciting motions for the robot trajectories [17, 18, 40]. It is important to minimize the computation time and maximize the collected information. The *log determinant* excitation criterion was applied. This criterion represents the optimal option with minimal error over a short time-period, according to the identification in real-time [34]. The optimization generates the constrained exciting motion with respect to the joint angles, velocities, accelerations, and torques within their physical limitations. Moreover, constraints to prevent auto-collision and collisions with the environment were included in the process.

5. Reference Motion Planning

In this work, the main task was the painting of flat surfaces with smooth and continuous trajectories. The task was conducted using different sizes of painting rollers.

Table 2. Physical parameters for the painting roller tools.

Name of the roller	*Length* [m]	*Width* [m]	*Weight* [kg]
Big roller	0.35	0.20	0.2
Small roller	0.33	0.10	0.1

Table 3. Identified inertial parameters for big and small rollers [34] (see Section 3.2 for the definition of each symbol).

Parameter	$\mathbf{\Phi}_{br}$	$\%\sigma_{\Phi_{br}}$	$\mathbf{\Phi}_{sr}$	$\%\sigma_{\Phi_{sr}}$
M [kg]	2.4×10^{-1}	0.5	9.7×10^{-2}	1.3
MSX [kgm]	-3.9×10^{-3}	8.1	4.5×10^{-5}	28.4
MSY [kgm]	-1.5×10^{-5}	21.0	7.2×10^{-5}	25.4
MSZ [kgm]	6.5×10^{-2}	0.6	2.4×10^{-2}	1.4
XX [kgm^2]	2.0×10^{-2}	1.9	7.4×10^{-3}	4.4
YY [kgm^2]	2.1×10^{-2}	2.0	7.1×10^{-3}	5.1
ZZ [kgm^2]	2.1×10^{-3}	14.9	1.5×10^{-4}	31.0
XY [kgm^2]	5.6×10^{-4}	56.6	2.0×10^{-4}	102.8
XZ [kgm^2]	6.3×10^{-4}	41.5	-4.2×10^{-4}	54.7
YZ [kgm^2]	8.3×10^{-5}	49.9	2.1×10^{-4}	47.5

Moreover, it required precision and adaptation in accordance with the changes in the physical parameters of the end-effector (painting rollers) of the robot. In particular, the robot manipulator traced a painting trajectory in the shape of "W" on the wall using painting rollers attached to the end-effector. The size of the "W" trajectory was approximately 0.2 m $\times$ 0.2 m. The painting roller was applied to the wall with a constant force of 30 N. In this work, two painting rollers (big and small) specified in Sections 4 and 7 (environmental setup) were used. The initial parameters are presented in **Tables 2** and **3** of the end-effector parameters. The trajectory for the painting task was generated in the Cartesian space by the optimization process [37]; thus ensuring a smooth trajectory and stability in the joints, in addition to a high-quality outcome of the final painting task.

The motion of the robot was designed for trajectories in the Cartesian space. The trajectories were planned via an optimization process with constraints, and the optimization generated the trajectories with conditions for smooth motions using the dynamic robot and end-effector identification.

The optimization for the motion trajectory minimizes a cost function constituted by the norm of the robot joint jerks and the duration of the desired trajectory. Simultaneously, the optimization maximizes the work area (in the case of a painting surface by the horizontal and vertical distances traveled by the roller) during the motion; thus ensuring dynamic and kinematic viability in the robot.

The Cartesian trajectory applied in this study was developed by T. Katsumata et al. [34]. It consists of a painting trajectory with six DoFs; $P_C = [\overline{P}_X \quad \overline{P}_Y \quad \overline{P}_Z \quad \overline{\theta}_X \quad \overline{\theta}_Y \quad \overline{\theta}_Z]^T$. It is described by the

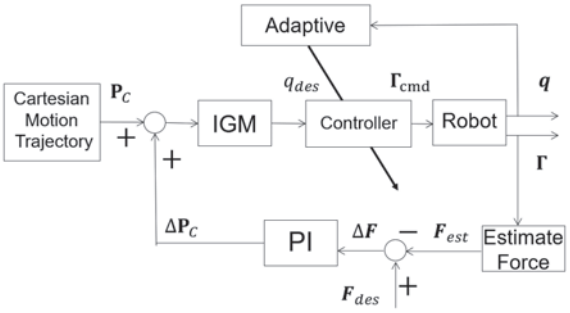

Fig. 4. Adaptive control system for robot force and position control based on fast dynamic and geometric identification.

3D positions $\overline{\mathbf{P}}_{X,Y,Z}$ of the end-effector and the orientations represented by Euler angles $\boldsymbol{\theta}_{X,Y,Z}$. The path planning optimization problem can be expressed as the solution of $\mathbf{X}_{opt} = [T_c \quad \varphi \quad Z_u \quad Z_l \quad Y_0 \quad \Delta Y] \in \Re^6$, where the T_c represents the trajectory duration time; φ is the swivel angle; Z_u and Z_l are the upper and lower vertical positions of the roller, respectively; Y_0 is the initial horizontal roller position; and ΔY is the horizontal distance traveled by the roller. The Cartesian velocity and acceleration were defined as null at each way point. The trajectory was interpolated using 5th order *B*-splines.

6. Robot Control System (Position and Force Controllers)

The robot control system was designed according to the scheme as shown in **Fig. 4**. The objective of the proposed adaptive predictive and force control was the execution of the painting task with redundant robots, using continuous trajectories in Cartesian space ensuring smooth motion, stability, non-vibration, and precision during the task.

The system consisted of a Cartesian motion trajectory, which is the optimal reference calculated in Section 5 to execute the painting task. The inverse geometric model (IGM) is the model that converts the Cartesian information in joint references for the joint robot controllers using the identified parameters. The controllers were developed for force and position regulation. The force controller was designed using the calculated estimate force and a proportional-integral (PI) controller in the Cartesian space. The position controllers were developed using the PD-gravitational compensator, GPC, and AGPC. Moreover, the above mentioned controllers make use of the models identified in the previous sections.

The control system performance was validated by analyzing the stability, robustness response, and precision of the trajectory tracking. In addition, the focus of this work was to determine the applicability of fast identification combined with the adaptation in robot control.

6.1. External Force Estimation

Applying the identification of the robot and of its end-effector, the external forces could be estimated from the measured joint torques using the following equations:

$$\begin{cases} \boldsymbol{\Gamma} = \widehat{\mathbf{M}}(\mathbf{q})\ddot{\mathbf{q}} + \widehat{\mathbf{C}}(\mathbf{q},\dot{\mathbf{q}}) + \widehat{\mathbf{G}}(\mathbf{q}) + \boldsymbol{\Gamma}_{ext} \\ \boldsymbol{\Gamma} = \boldsymbol{\Gamma}_{dyn} + \boldsymbol{\Gamma}_f + \boldsymbol{\Gamma}_{ext} \\ \mathbf{F}_{est} = (\mathbf{J}^T)^+ \boldsymbol{\Gamma}_{ext} \mathbf{F}_{est} = (\mathbf{J}^T)^+ (\boldsymbol{\Gamma} - \boldsymbol{\Gamma}_{dyn}) \end{cases} . \quad (5)$$

where $\mathbf{J}$ is a (6×7) robot Jacobian matrix; $\widehat{\mathbf{M}}(\mathbf{q})$ (7×7) is the identified robot inertia matrix; $\widehat{\mathbf{C}}(\mathbf{q},\dot{\mathbf{q}})$ (7×1) is the vector that contains the identified Coriolis and centrifugal terms; $\boldsymbol{\Gamma}$ and $\boldsymbol{\Gamma}_{dyn}$ are the measured and estimated joint torques, respectively; and $\mathbf{F}_{est}$ (6×1) is the estimated vector of the external forces in Cartesian space.

6.2. Force Control

The proposed control scheme is composed of two embedded control loops [41]. The outer loop controls the external forces, and the inner loop controls the pose of the Cartesian end-effector as shown in **Fig. 4**. The additional displacement to the desired Cartesian 3D position, due to the force control, is given by:

$$\Delta P_C = \mathbf{K}_p^f (\mathbf{F}_d - \mathbf{F}_{est}) + \mathbf{K}_i^f \int_{T_0}^{T} (\mathbf{F}_d - \mathbf{F}_{est}) \quad . \quad . \quad (6)$$

where ΔP_C is the additional displacement reference signal in Cartesian space; $\mathbf{F}_d$ is the desired external force; $\mathbf{K}_p^f$ and $\mathbf{K}_i^f$ are the proportional and the integral gains, respectively; and T_0 and T represent the initial time and current time, respectively.

6.3. Position Control

For the position control of the painting motion, several control techniques were developed using the previously calculated identification models. First, a PD control with a gravitational compensator was proposed. Second, a PD control with feedforward compensation was developed. Finally, GPC and AGPC were proposed.

6.3.1. PD control & Gravitational Compensator

The PD control with a gravitational compensator was designed by tuning the gains as a classical joint space PD controller [42] with P gain $[1500, 5000, 1000, 2000, 500, 200, 200]$ and D gain $[50, 50, 30, 30, 20, 10, 10]$ for links 1–7, respectively. The gravitational torque was computed using the dynamic parameters identified in the previous part. Given that the dynamic models of the robot and painting tool were already identified, the PD control could be expressed as:

$$\Gamma_d = \mathbf{K}_p(\mathbf{q}_d - \mathbf{q}) + \boldsymbol{K}_d(\dot{\mathbf{q}}_d - \dot{\mathbf{q}}) + \widehat{\mathbf{G}}(\mathbf{q}) \quad . \quad . \quad . \quad (7)$$

where $\mathbf{K}_p$ and $\mathbf{K}_d$ are $(N_J \times N_J)$ diagonal matrices for the experimentally-tuned proportional and derivative gains; $\mathbf{q}_d$ (7×1) and $\dot{\mathbf{q}}_d$ (7×1) are the vectors of the desired and measured joint angles, respectively; $\dot{\mathbf{q}}_d$ and $\dot{\mathbf{q}}$ were obtained by the first-order backward difference with respect to $\mathbf{q}_d$ and $\mathbf{q}$; and $\widehat{\mathbf{G}}(\mathbf{q})$ $(N_J \times 1)$ is the vector of gravitational terms obtained using the identified inertial parameters.

6.3.2. PD Control and Feedforward

The PD control with feedforward was applied, as expressed in Eq. (8). Typically, the plant with previous determined dynamics and a predefined trajectory was controlled using feedback and feedforward controls. The feedforward torques were computed using the identified dynamic parameters and dynamic model of the robot. Moreover, P gains and D gains were tuned using the same values of the PD gravitational compensator control.

$$\begin{aligned}\boldsymbol{\Gamma}_d &= \mathbf{K}_p(\mathbf{q}_d - \mathbf{q}) + \mathbf{K}_d(\dot{\mathbf{q}}_d - \dot{\mathbf{q}}) \\ &\quad + \widehat{\mathbf{M}}(\mathbf{q})\ddot{\mathbf{q}} + \widehat{\mathbf{C}}(\mathbf{q}_d, \dot{\mathbf{q}}) + \widehat{\mathbf{G}}(\mathbf{q}_d) \quad . \; . \; . \; . \; . \; (8)\end{aligned}$$

6.3.3. Generalized Predictive Control (GPC)

The generalized predictive control scheme was applied for the position control, to improve the performance of the robot with respect to its trajectory tracking with predictive actions, velocity, precision, and stability. Before describing the GPC design, the linearization method is presented. In this study, the same feedback linearization technique as that in the common case of computational torque control (CTC) was used [43] to calculate suitable models for the design of the predictive controllers. The nonlinear dynamic model of the robotic arm was considered, as expressed in Eq. (1). That robotic arm equations could be linearized and decoupled by nonlinear feedback, as expressed by

$$\boldsymbol{\Gamma} = \widehat{\mathbf{M}}(\mathbf{q})\mathbf{w} + \widehat{\mathbf{C}}(\mathbf{q}, \dot{\mathbf{q}}) + \widehat{\mathbf{G}}(\mathbf{q}) \quad . \; . \; . \; . \; . \; . \; (9)$$

$\widehat{\mathbf{M}}(\mathbf{q})$, $\widehat{\mathbf{C}}(\mathbf{q}, \dot{\mathbf{q}})$, and $\widehat{\mathbf{G}}(\mathbf{q})$ are the estimates of $\mathbf{M}(\mathbf{q})$, $\mathbf{C}(\mathbf{q}, \dot{\mathbf{q}})$, $\mathbf{G}(\mathbf{q})$, respectively; and $\mathbf{w}$ is the new input control vector. Assuming that $\widehat{\mathbf{M}}(\mathbf{q}) = \mathbf{M}(\mathbf{q})$, $\widehat{\mathbf{C}}(\mathbf{q}, \dot{\mathbf{q}}) = \mathbf{C}(\mathbf{q}, \dot{\mathbf{q}})$, and $\widehat{\mathbf{G}}(\mathbf{q}) = \mathbf{G}(\mathbf{q})$ the problem is reduced to a linear and decoupled double-integrators system, where N is the number of DoFs of the robot [44].

$$\ddot{\mathbf{q}} = \mathbf{w} \quad . \; . \; . \; . \; . \; . \; . \; . \; . \; . \; . \; . \; . \; . \; . \; . \; . \; . \; (10)$$

Furthermore, Eq. (10) corresponds to the inverse dynamic control scheme, where the dynamics of the robot are transformed into a double set of integrators. Thus, linear control techniques can be used to design position-tracking controllers such as the model-based predictive control (i.e., GPC). Moreover, the GPC is a type of model predictive control algorithm. Predictive control can be summarized as follows [22, 45]: 1) the definition of a numerical model of the system to predict future behavior; 2) the minimization of a quadratic cost function over a finite future horizon using future predicted errors; 3) the elaboration of a sequence of future control values by applying the first value to the system and the model; and 4) the iteration of the entire procedure during the next sampling period, according to the "receding horizon" strategy [23]. For the GPC, the plant was modeled using controlled autoRegressive moving average (CARIMA) model (Eq. (11)). Moreover, $A(z^{-1})$ and $B(z^{-1})$ polynomials were obtained by discretizing the linearized model (Eq. (10)), and $C(z^{-1})$ is the polynomial with coefficients that represent the white noise in the system.

$$A(z^{-1})y(t) = B(z^{-1})u(t-1) + \frac{C(z^{-1})}{\Delta}\xi(t) \quad . \; (11)$$

where $u(t)$ and $y(t)$ are the plant input and output respectively; and $\xi(k)$ is a centered Gaussian white noise.

The optimal predictor (Eq. (12)) was configured with the matrix in the past, present, and future actions of $F_j(z^{-1})$, $H_j(z^{-1})$, and $G_j(z^{-1})$, respectively [25].

$$\begin{aligned}\hat{y}\left(t + \frac{j}{t}\right) &= \frac{F_j(z^{-1})}{C(z^{-1})}y(t) + \frac{H_j(z^{-1})}{C(z^{-1})}\Delta u(t-1) \\ &\quad + G_j(z^{-1})\Delta u(t+j-1) \quad . \; . \; . \quad (12)\end{aligned}$$

Equation (12) can be written in the following vector form:

$$\widehat{\mathbf{y}} = \frac{1}{C(z^{-1})}\mathbf{if}y(t) + \frac{1}{C(z^{-1})}\mathbf{ih}\Delta u(t-1) + \mathbf{G}\tilde{u} \quad (13)$$

where

$$\left\{\begin{array}{l} \mathbf{if} = [F_{N1}(z^{-1}), \ldots, F_{N2}(z^{-1})]^T \\ \mathbf{ih} = [H_{N1}(z^{-1}), \ldots, H_{N2}(z^{-1})]^T \\ \tilde{\mathbf{u}} = [\Delta u(t), \ldots, \Delta u(t+N_u-1)]^T \\ \widehat{\mathbf{y}} = [\hat{y}(t+N_1), \ldots, \hat{y}(t+N_2)]^T \\ \mathbf{r} = [r(t+N_1), \ldots, r(t+N_2)]^T \\ \mathbf{G} = \begin{bmatrix} g_{N1-1} & \cdots & g_0 & 0 & \cdots & 0 \\ g_{N1} & \cdots & g_1 & g_0 & \cdots & 0 \\ \vdots & \ddots & \vdots & \ddots & \ddots & \vdots \\ g_{Nu-1} & \cdots & \cdots & \cdots & \cdots & g_0 \\ \vdots & \ddots & & & & \vdots \\ g_{N2-1} & \cdots & \cdots & \cdots & \cdots & g_{N2-Nu} \end{bmatrix} \end{array}\right. \quad . \; . \; (14)$$

Each element of the $\mathbf{G}$ matrix represents the dynamic response of the system. The control signal Δu was obtained by minimizing of the quadratic cost function (Eq. (15));

$$\begin{aligned}J &= \sum_{j=N_1}^{N_2}\left([\hat{y}(t+j|t) - w(t+j)]^2\right) \\ &\quad + \sum_{j=N_1}^{N_u}\left(\lambda(j)\,[\Delta u(t+j-1)]^2\right) \quad . \; . \; . \; . \; (15)\end{aligned}$$

where N_1 and N_2 define the range of the prediction output, N_u defines the control horizon, λ is a control weighting factor, $r(k)$ is the reference value, $y(k)$ is the prediction output value obtained by solving the Diophantine equation, and Δu is the control signal. Moreover, Eq. (15) can be expressed by a vector with the following form:

$$J = (\widehat{\mathbf{y}}(t) - \mathbf{r}(t))^T(\widehat{\mathbf{y}}(t) - \mathbf{r}(t)) + \Delta\mathbf{U}(t)^T\Lambda\Delta\mathbf{U}(t) \quad (16)$$

where

$$\left\{\begin{array}{c} \Lambda = \mathrm{diag}[\lambda(1), \ldots, \lambda(N_u)] \\ \Delta\mathbf{U}(t) = [\Delta u(t), \ldots, \Delta u(t+N_u-1)]^T \end{array}\right. \quad . \; . \; (17)$$

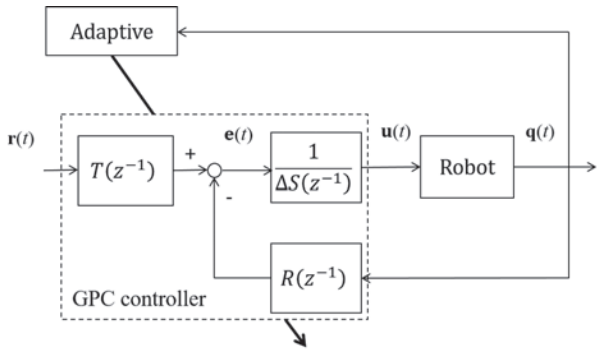

Fig. 5. Scheme for the AGPC.

By substituting Eq. (13) into Eq. (16) and partially differentiating $\Delta\mathbf{U}(t)$, the control law $\tilde{u}_{opt}$ that minimizes the evaluation function (Eq. (18)) was obtained as follows:

$$\tilde{u}_{opt} = -\mathbf{N}\left[\frac{1}{C(z^{-1})}\mathbf{if}y(t) + \frac{1}{C(z^{-1})}\mathbf{ih}\Delta u(t-1) - \mathbf{r}\right] \quad (18)$$

where

$$\begin{cases} \tilde{u}_{opt} = [\Delta u(t)_{opt}, \ldots, \Delta u(t+N_u-1)_{opt}]^T \\ \mathbf{N} = [\mathbf{G}^T\mathbf{G} + \Lambda]^{-1}\mathbf{G}^T = \begin{bmatrix} \mathbf{n}_1^T \\ \vdots \\ \mathbf{n}_u^T \end{bmatrix} \end{cases} . \quad (19)$$

The receding horizon principle assumes that only the first value of the optimal control series $\tilde{u}_{opt}$ is applied; thus for the next step, the procedure is repeated. Finally, the GPC is expressed as shown in Eq. (20):

$$\Delta u(t) = -N_1^T\left[\frac{1}{C(z^{-1})}\mathbf{if}y(t) + \frac{1}{C(z^{-1})}\mathbf{ih}\Delta u(t-1) - \mathbf{r}\right] \quad (20)$$

The design was therefore implemented adjusting T_s, N_1, N_2, N_u, and λ to satisfy the required input/output behavior, i.e., fastest response that is consistent with the stability requirements. With this control strategy, a two-DoF reference signal tracking (RST) controller was obtained, and the procedure is described in [46, 47]. The resulting GPC was then synthesized as a two-DoF controller, as shown in Eq. (21).

$$S(z^{-1})\Delta u(t) = -R(z^{-1})y(t) + T(z)w(t+N_2) \quad . \quad . \quad (21)$$

The controller was calculated using synthesized polynomials $R(z^{-1})$, $S(z^{-1})$, and $T(z^{-1})$.

6.3.4. Adaptive GPC

The AGPC was also implemented for position control, and the structure is presented in **Fig. 5**. In the real-time robot manipulation case, it may be difficult to obtain reliable acceleration information. In particular accurate acceleration information could not be obtained when the previous experiment with the real robot was conducted in this study. Without the acceleration information, advanced control techniques such as CTC could not be applied to the system. Consequently, the adaptation of the GPC was designed using the dynamic information of the robot, and the robot modeling varied in accordance with the new robot states. The AGPC then tunes its parameters on-time based on the posture of the robotic arm, and directly calculates the control signal without a decrease in the performance of the robot. This automated design process simplifies the tuning process, thus increasing the versatility of the proposed system in that it can be applied to any serial robotic arm. According to Khalil and Dombre [44], the approximate dynamic model of robot arm links can be expressed as a linear second order differential equation:

$$\Gamma_j = m_j\ddot{q}_j + F_{vj}\dot{q}_j + \gamma_j \quad . \quad . \quad . \quad . \quad . \quad . \quad . \quad . \quad . \quad (22)$$

where $m_j = M_{jjmax}$ is the maximum magnitude of element M_{jj} of the inertial matrix of the robot, γ_j represents a disturbance torque, and F_{vj} is the coefficient of viscous friction.

The inertial characteristics of the robot vary in accordance with the motions of the robot; thus, the variations and the differences between the real dynamics and approximate dynamic model may result in unstable control. Therefore, to stabilize the GPC, the update of $R(z^{-1})$, $S(z^{-1})$, and $T(z^{-1})$ polynomials was attempted, due to the adaptive optimization with respect to the current robot motion. Moreover, the AGPC was stabilized by adjusting the GPC design parameter λ and final horizon N_2.

The controller directly adapts the control parameters from the optimal design in an on-line scheme. Two main optimization procedures are executed during the adaptation of the controllers. The first is the calculation of the optimal weight control λ and the predictive window for the control design, which are based on the minimum receding horizon, minimum time, and stability response as the main constraints in the optimization problem. The second optimization is executed to determine the optimal predictive controllers based on the optimal variables, to obtain the polynomials that produced the robot torques for each joint.

The optimization to determine the optimal parameters (weight for control input λ and predictive window N_1–N_2) is based on the stability analysis, according to the dynamic models and the predictive laws, as discussed in Sections 6.3.3 and 6.3.4. For the stability analysis, the phase and gain margins are calculated. The phase margin is required to be larger than 45°, and the gain margin is required to be larger than 6 dB, to be selected as the optimal controller. The stability analysis is conducted every 0.1 s to determine the optimal λ for the GPC. The initial optimal λ is calculated using the solution of the Diophantine equation and the matrix in Eq. (14). The optimal λ is selected based on the λ that yields the best stability response. Every choice of λ is evaluated with respect to the system stability. The corresponding λ is selected as the new optimal λ until the next time-period. Currently, the algorithm is set to select the best λ from 20 sets in the range of $0.01 \sim 5.0 \times 10^8$. Besides λ, N_2 is preferred to

be small, as it has a direct influence on the computational cost and delay of the system response. On the other hand, a larger N_2 generally results in an increased system stability. In this study, the initial value of N_2 was set as a minimum and tolerable value of the gain and phase margins, and to provide the stable regulators expressed in Eqs. (20) and (21). The stability analysis was conducted over the entire duration of the task. Moreover, if the λ cannot provide system stability, the algorithm immediately changes the final window of predictor N_2, and a new λ is selected. Furthermore, the optimal parameters are validated using the robustness criteria, which involves checking the direct and complementary sensibilities in Eq. (23). With this λ, the design of the controllers ensures that the robot action is sufficient to maintain stable actions during the painting task.

The adaptive algorithm is summarized below.

1. Calculate the inertial matrix of the robot at the sample time using the angle information and identified dynamic parameters.

2. Build the new robot models for each link using the updated information of the dynamic model (Eq. (22)) of the robot.

3. To determine the first optimal predictor, design the GPC controllers with the initial setup of the parameters: the prediction horizon N_1, N_2, the control horizon N_u, and the sample time T_s.

4. Execute the optimization process using the minimization of the cost function represented in (Eq. (15)) and the resolution of the Diophantine equation, to obtain the possible regulators for multiple options of the weighting parameter λ and extended horizon N_2. The optimization can be configured by a time cycle (defined by the user, and related to the desired robot velocity), and it is associated with the prediction time-period. Moreover, it determines the final N_2 prediction horizon, executes different options, and starts with the stable N_2 until the final cycle time. This step enables the analysis of the stability for different optimal λ and the extended horizon N_2 values. Moreover, it determines the minimum final horizon that is suitable for the high velocity robot motion.

5. The values of N_2 and λ are selected with the minimum extended horizon.

6. Using the response of the 5th step, a second optimization with a new horizon N_2 is calculated using Eqs. (17) and (18), to obtain the updated optimal λ.

7. The results of the 6th step are used to compute the stability margin gains of each GPC controller using the final optimal parameter λ and N_2.

8. The optimal GPC controllers for all the links are determined based on the stability results from the temporal and frequency analysis. The robustness of the controllers is analyzed using the direct and complementary sensibility of the robot with the new controllers (Eq. (23)). The results of GPC controllers for each of the joint polynomials $R_0(z^{-1})$, $S_0(z^{-1})$, $T_0(z^{-1})$ are configured with the optimal parameters, and then validated with respect to the stability and robustness using the frequency response of the robot. Bode and black analyses reveal the relationship between the measurement of the direct sensitivity σ_d, and the complementary sensitivity σ_c. The first represents the relationship between the output and the noise measurement, and the second represents the relationship between the output and the perturbation in the robot when the AGPCs are applied.

$$\begin{cases} \sigma_d = \dfrac{A(z^{-1})\Delta S(z^{-1})}{A_c(z^{-1})C(z^{-1})}, \\ \sigma_c = \dfrac{(z^{-1})B(z^{-1})R(z^{-1})}{A_c(z^{-1})C(z^{-1})} \end{cases} \quad \ldots \quad (23)$$

9. Using the response of the 8th step, the Δu control signal (Eq. (20)) is synthesized by the adaptive polynomials $R_{adp}(z^{-1})$, $S_{adp}(z^{-1})$, and $T_{adp}(z^{-1})$, to send the direct torques command for the robot.

10. The control is then continued until the next sample time comes.

11. Return to the 1st step.

The stability analysis is conducted over the entire duration of the task, and the optimal λ is selected by the algorithm. If the algorithm cannot determine the optimal λ that can yield a sufficient system, it immediately changes the final window of the predictor N_2 and starts searching for a new λ.

The main differences between the GPC + feedback linearization and AGPC are the presence of the linearizer and the adaptive method used to develop the on-line optimization for the control design parameters and final controllers. The GPC + feedback linearization uses a strict linearizer to reduce the controlled system, as shown in Eq. (10). However, the linearizer is sensitive to model errors such as the mass of the end-effector; thus, the model error affects the entire linearizer, and the GPC is optimized using the linearizer for the controlled system. Model errors therefore decrease the control performance. On the other hand, the AGPC is designed to be stable at all times by analyzing the system responses throughout the duration of the task. Moreover, it guarantees a certain range of robustness against model errors. Thus, the AGPC is less sensitive to the model errors than the GPC. In addition, the AGPC is an auto tuning system; thus, the user is not required to determine optimal set of design control parameters such as in the case of the GPC + feedback linearization. Although GPC + feedback linearization demonstrated an improved tracking ability and lower computation cost, AGP exhibited a superior

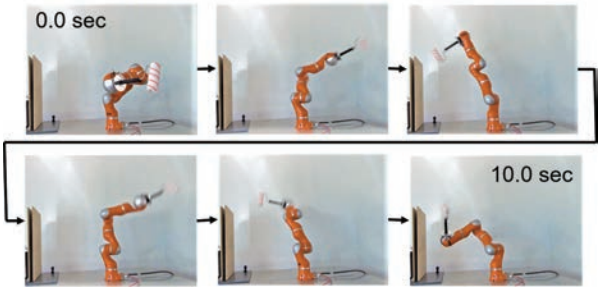

Fig. 6. Robot motion for dynamic identification with optimal exciting trajectories [34].

control performance. Moreover, it confirmed the potential of the GPC adaptation in the application with the online robotic arm during the task. The performance of the proposed AGPC therefore verified the effectiveness of the GPC solving the robotic arm control problem using a simple model such as in Eq. (22), and demonstrated the robustness and applicability of the GPC scheme.

7. Experimental Setup

The position and force controllers with the proposed adaptive predictive control scheme were validated using the KUKA LWR real experimental identification data [34], models, MATLAB, SYMORO+ [36], and V-REP simulation platforms. For the experimental identification, the KUKA LWR was working on a custom-built painting wall (height: 0.8 m, width: 0.6 m). A six-axes force sensor (ATI, Mini45) was employed to measure the reference force data, and it was positioned at the center of the wall. The desired external forces were set as F_d equal $(-30, 0, 0)$ N. **Fig. 6** presents the KUKA environment when the exciting motion was executed for the identification of the parameters.

The identification and control were validated using two different types of painting rollers. **Table 2** presents the physical parameters of these tools, and **Table 3** presents the identified parameters.

The dynamic identification of the end-effector using different painting rollers was implemented using a model discussed in Section 4. The identification was conducted by analyzing the relationship between the geometric and inertial parameters. In particular, the value of the inertial parameters increases in accordance with the size of the tool. The identified moment of inertia around the two axes were larger than the remaining axis [37]; thus, the physical parameters of different tools could be determined using a look-up table, as explained in Section 4, in addition to conducting PCA method to recognize between the characteristics of the tools and that of other tools.

The KUKA LWR used in this study had a mass of 12 kg, and the masses of the rollers were $100 \sim 200$ g. Although the differences between the masses of the rollers were relatively small, and a difference of 100 g could affect the control system as it attempts to conduct precise and high-speed tasks, more over with paint the wait of the roller may be double or triple. It should be noted that the proposed system successfully identified the physical parameters of the rollers and discriminate between the different rollers, although the mass difference between the rollers was only 0.1 kg. Furthermore, the identified values were used to implement the model predictive control such as the GPC and AGPC, to provide a superior control performance to that of the PD + Grv control.

The masses and dimensions of the rollers were linked in the look-up table and updated for the final robot models. Moreover, they were used for the GPC controllers and the computation of the gravitational compensation torque for the PD + Grv control. The models were modified specifically in the control torque described in Eqs. (7)–(9) and (22). If there were any changes in the physical parameters of the roller, the identification could solve the new parameters and update the models for the controllers.

Table 3 presents the values of the identified inertial parameters for both paint rollers. It can be considered the two identified masses are closed to their reference one. The parameters were downsized using PCA and stored in a look-up table with associated geometric parameters. Thus, the robot could recognize the painting roller attached to the end-effector. These values were obtained in the previous experimental identification developed by the authors of this paper in [34], using the data of the joint angles and torques when the optimal exciting motions were applied at 1 kHz. The root mean square (RMS) obtained with this identification was $J_d = 0.63$ Nm.

8. Results and Discussion

8.1. Position and Force Control Results

Using the complete experimental identification models, the controllers were implemented on a platform in which other types of robots and controllers could be configured. To validate the proposed approach, the painting trajectory was executed using a classical position/force controller, as presented in **Fig. 4**. The position and force control was performed using the PD controller with gravitational compensation in the real robot, in addition to the identified models. Subsequently, the predictive controllers of the position and force control were implemented on the platform. **Fig. 7** presents the desired painting trajectory generated by the optimization process [34] using the identified models in both roller cases. By identifying the dynamic and geometric models, a painting trajectory that satisfied the dynamic robot limitations could be generated from the updated models. Given that the masses of the end-effectors were low, the painting trajectories were remarkably similar. However, the advantage of the proposed method can be clearly seen in the case of a heavy payload. The real-time duration of each trajectory was 50 s and 46 s for the large roller and small roller, respectively.

For the force control, the estimated external force was

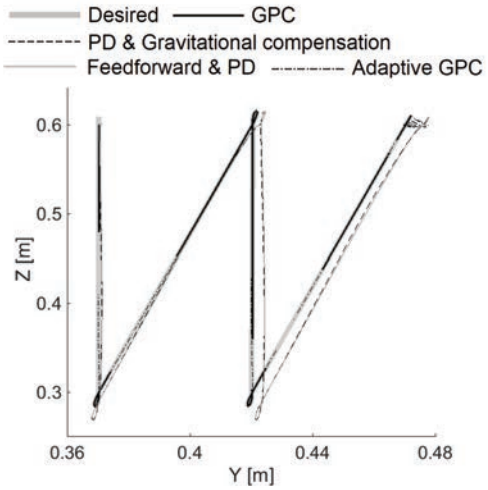

Fig. 7. Results with GPC, AGPC, and PD+ for small roller.

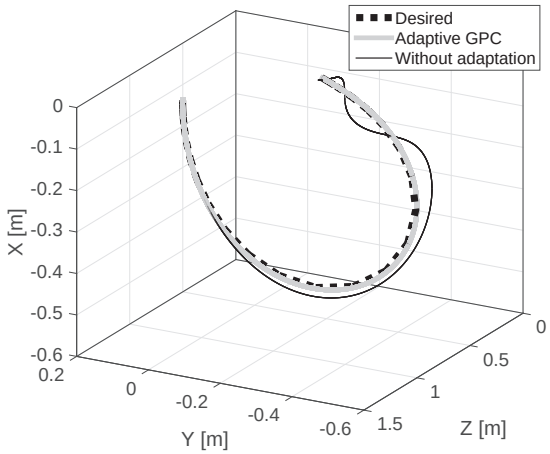

Fig. 8. 3D trajectory result with AGPC controller.

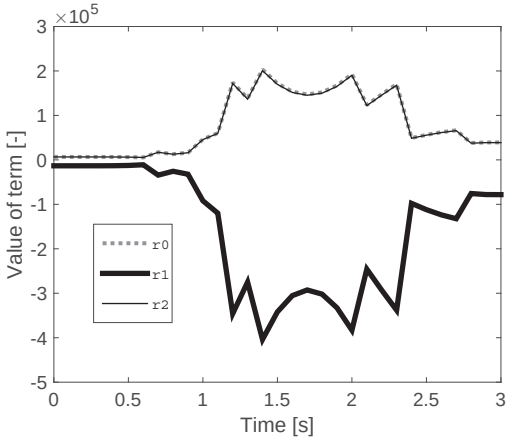

Fig. 9. Transition of $R(z^{-1})$ polynomial terms r_0, r_1, and r_2 with respect to the new optimal λ.

used in the control feedback. The corresponding differences in the RMS (NRMS) values between the estimated force and measured external force were 2.9 Nm (9.8%) and 2.0 Nm (6.8%) for the big roller and small roller, respectively. From the results, it is evident that the controller can adequately control the estimated external force using the feedback of the external forces that was estimated without force sensors (RMS error $\leq$ 3 N). Besides the force control, there was approximately 5 mm of a constant position error in the tracking control with the PD controller and gravitational compensation in the cases of the big roller and small roller.

8.2. GPC, AGPC, and PD+ Gravitational Controllers Results

Although the system demonstrated a sufficient force control and tracking control performance, a constant position error of approximately 5 mm was presented in each case, as mentioned above. The error may be suitable for the painting task over a large area. However, the system would be required to reduce the position error if the complexity of the task and precision requirements increased such as writing small letters or locate the tool into the reduced place. Therefore, other controllers with the adaptive methods for position error were proposed, i.e., the GPC, AGPC, and feedforward-PD control using the optimal trajectory and force control strategy discussed in the previous sections.

To ensure the proper functioning of the AGPC, simple motion control was conducted using the AGPC in the V-REP environment. **Fig. 8** reveals that the AGPC could stably control the LWR and follow the reference with minimal error. Moreover, **Fig. 9** presents an example of the polynomial $R_{adp}(z^{-1})$, and how it varied in accordance with changes in the posture of the robot.

Figures 7–12 show that the GPC and AGPC controllers yielded accurate tracking, whereas the PD control-gravitational compensation and feedforward-PD control deviated from the desired trajectory, as the painting motion progressed. Given that the PD and feedforward control do not support integral action, the robot could not handle the position error caused by the external force at the end-effector. On the other hand, the GPC supports integral action due to the nature of its structure, successfully managed the disturbance of external force and exhibited a significant improvement of tracking ability.

Furthermore, the results reveal that the GPC with feedback linearization demonstrates a good performance due to the fine identified inertial parameters used to develop the model of the robot. **Fig. 13** presents the RMS position error when the controllers were implemented. The GPC and AGPC yielded a minimal position error when compared with that of PD with gravitational compensation. The results for the GPC and AGPC were 0.1 mm and 0.21 mm with the small roller, and 0.22 mm and 0.62 mm with the big roller in the end-effector, respectively.

As shown in **Figs. 14** and **15**, the GPC and AGPC yielded better force control results due to their fast reaction capabilities. The AGPC presented a better control result than the adaptive PD control with gravitational com-

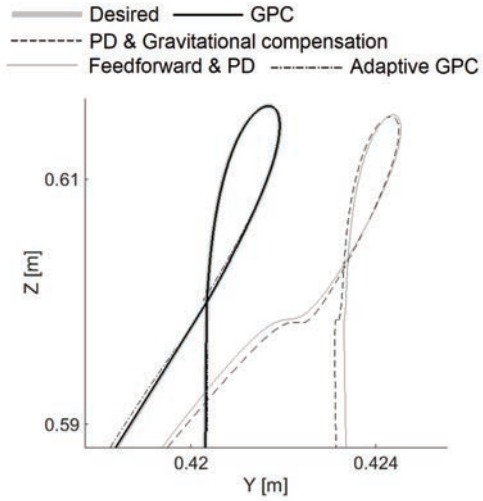

Fig. 10. Zoom result for small roller with GPC, AGPC, and PD+.

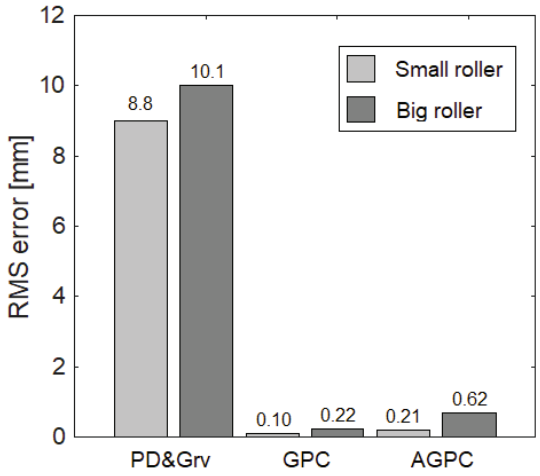

Fig. 13. RMS position error with GPC, AGPC, and PD controllers.

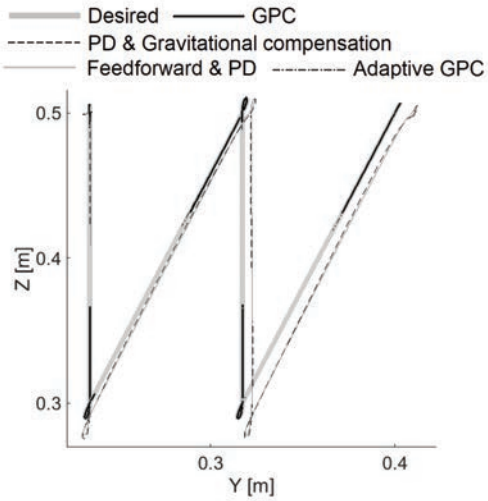

Fig. 11. Results with GPC, AGPC, and PD+ for big roller.

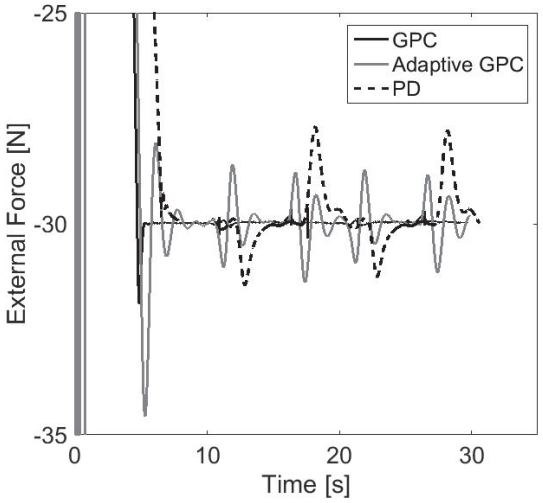

Fig. 14. External Force with GPC, AGPC, and PD controllers.

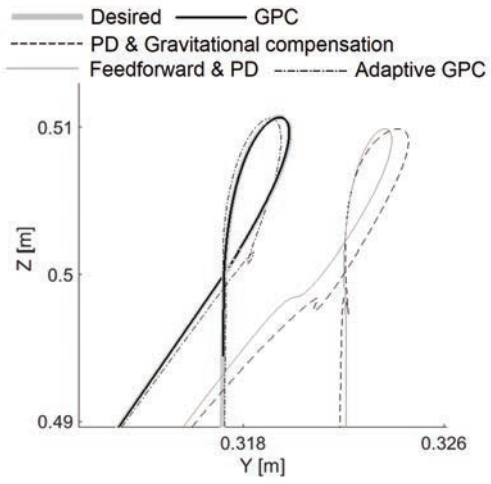

Fig. 12. Zoom results for big roller with GPC, AGPC, and PD+.

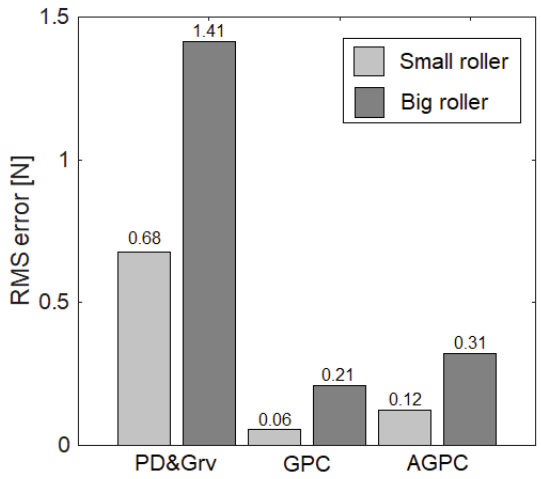

Fig. 15. RMS force error with GPC, AGPC, and PD controllers.

pensation. Moreover, the AGPC re-adjusted according to the posture of the robot arm on-line, and its automated tuning structure reduced the initial tuning process when it was implemented in other robotic arms. In addition, in the case of the GPC with feedback linearization, the AGPC can affect directly the signal control with the acceleration feedback, which could contain a noise error in the real situation. Thus, the AGPC is more suitable for robots in planning and motion tasks.

The performance of the GPC was stable and precise during the trajectory tracking. Moreover, it was robust with respect to changes in the end-effector. However, it could not adapt to new changes during the execution of the task, and the variability of the rollers when exposed to new elements or environments.

Table 4. Computational cost using the GPC, AGPC, and PD+ during the painting task.

Controller	*Memory* [GB]	*%CPU*	*CPUtime* [s]
AGPC (small roller)	0.993	27	0.043
AGPC (big roller)	0.628	21	0.051
GPC (small roller)	0.950	23	0.032
GPC (big roller)	0.599	21	0.040
PD+ (small roller)	0.628	18	0.037
PD+ (big roller)	0.601	17	0.038

8.3. Considerations of the Controllers

The GPC developed in this study implemented the feedback linearization, and was optimized by tuning the parameter λ, prediction windows N_1–N_2, and control horizon N_u, as discussed in Section 6.3. The parameters were previously set to start the motion control. By adjusting the parameters, GPC response speed, and convergence speed/position, the stability and robustness sensibilities changed. Given that the controlled system is strictly linearized, and that its controlled system does not change over the range of motion, a fixed GPC (fixed values of design parameters) is applicable to this system, and the values of the optimal parameters depend on the robot dynamics and motion task.

By combining GPC + feedback linearization and on-line system identification, another AGPC can be introduced. Using on-line system identification, the system could detect whether the robot is in high-speed motion or interacting with the external environment. In this case, the high response speed of the GPC should be designed by adjusting the design parameters. Moreover, it is possible that using on-line system identification to design the feedback linearizer on-line strictly linearizes the robot system. This system identifies the dynamic parameters of the robot on-line and simultaneously constructs a feedback linearizer using the identified values. Eventually, the optimal linearizer is obtained by evaluating the tracking error. However, it is difficult to set the initial parameters for the linearizer and the GPC, which provide a certain level of stability from the start of the motion.

Once the dynamic and geometric parameters are identified, the integration with the GPC + feedback linearization in on-line system identification is applicable to the robot for the generation of an adaptive optimal predictor. In this case, the feedback linearization could calculate new models and modify the optimal predictor. The controller could then be enhanced by considering the contribution of the AGPC scheme proposed in this paper by calculating the optimal on-line control parameters based on the dynamic and geometric identification.

The computational cost was calculated by the program for different types of rollers, to validate the GPC, AGPC, and PD+ controllers. The computational cost was verified by measuring the allocated memory, % of CPU, and time consumption. The results are summarized in **Table 4**.

The table above presents CPU time of each controller for one cycle. As expected, it shows that the AGPC has the highest computational cost. This is because the AGPC conducts optimizations and stability analyses, in addition to the calculation of the control torques. In this study, the sampling time for the calculation was 1 ms; approximately 43 s was required to calculate 1 s of motion. However, this type of on-line adaptive controller can be further enhanced with potential computational characteristics to decrease the duration of the control tasks.

9. Conclusion

In this study, a novel robot control adaptation based on predictive controllers and the fast dynamic and geometric identification of base parameters in a force control framework was developed. The proposed methods were applied to the KUKA lightweight robot. During the roller painting task, the external forces applied to the end-effector could be estimated and controlled without a force sensor mounted at the end-effector, due to the accurate model identification. Moreover, the controllers were developed using the identification performed with the exciting motion of 10 s, which was generated by an optimization. The proposed adaptive predictive controllers were compared with other controllers such as the PD control with gravitational compensation, feedforward with PD control, and GPC. The AGPC updated itself during the motion and successfully controlled the robot with good stability by exploiting the fine identified SIPs. The GPC and AGPC demonstrated excellent control performances such as a 90% reduction in the position errors when compared with the results of the previous experiment. Moreover, a novel tuning design with robust control will be developed in the future to enhance the AGPC. Furthermore, the future work will extend this method to a significantly larger number variables, rollers, and tools.

Acknowledgements

This research was pertly supported by the JSPS Grant in Aid [grant number K102604768], and the Japan Student Service Organization (JASSO) Student Exchange Support Program.

References:

[1] I. Iglesias, M. A. Sebastian, and J. E. Aresc, "Overview of the State of Robotic Machining: Current Situation and Future Potential," Procedia Engineering, Vol.132, pp. 911-917, 2015.

[2] T. Brogardh, "Identification and Control. Robot Control Overview: An Industrial Perspective," Modeling, Identification and Control, Vol.30, No.3, pp. 167-180, 2009.

[3] A. B. Moniz and B. J. Krings, "Robots Working with Humans or Humans Working with Robots? Searching for Social Dimensions in New Human-Robot Interaction in Industry," Societies, Vol.6, No.3, 2016.

[4] A. Albu-Schäffer, S. Haddadin, C. Ott, T. Wimbock, and G. Hirzinger, "The DLR Lightweight Robot: Design and Control Concepts for Robots in Human Environments," Indusrial Robot: An International J., Vol.34, No.5, pp. 376-385, 2007.

[5] M. H. Raibert and J. J. Craig, "Hybrid position/force control of manipulators," J. of Dynamic Systems, Measurement, and Control, Vol.103, pp. 126-133, 1981.

[6] A. Wahrburg, S. Zeiss, B. Matthias, and H. Ding, "Contact force estimation for robotic assembly using motor torques," 2014 IEEE Int. Conf. on Automation Science and Engineering (CASE), pp. 1252-1257, 2014.

[7] E. de Sol, R. King, R. Scott, and M. Ferre, "External force estimation for teleoperation based on proprioceptive sensors," Int. J. of Advanced Robotic Systems, DOI: 10.5772/58468, 2014.

[8] M. Linederoth, A. Stolt, A. Robertsson, and R. Johansson, "Robotic force estimation using motor torques and modeling of low velocity friction disturbances," IEEE/RSJ Int. Conf. on Int. Robots and Systems, pp. 3550-3556, 2013.

[9] K. S. Eom, I. H. Suh, W. K. Chung, and S. R. Oh, "Disturbance observer based force control of robot manipulator without force sensor," IEEE Int. Conf. on Robot. Autom., pp. 3012-3017, 1998.

[10] A. Alcocer, A. Robertsson, A. Valera, and R. Johansson, "Force estimation and control in robot manipulators," IFAC Symp. on Robot Control, pp. 31-36, 2003.

[11] Z. Liu, F. Yu, L. Zhang, and T. Li, "Real-Time Estimation of Sensor-Less Planar Robot Contact Information," J. Robot. Mechatron., Vol.29, No.3, pp. 557-565, 2017.

[12] Y. Fujimoto, S. Obata, and A. Kawamura, "Robust biped walking with active interaction control between foot and ground," IEEE Int. Conf. on Robot. Autom., pp. 2030-2035, 1998.

[13] M. Gautier and W. Khalil, "On the identification of inertial parameters of robots," IEEE Int. Conf. on Decision Control, pp. 2264-2269, 1998.

[14] W. Khalil and E. Dombre, "Identification of the dynamic parameters," "Modeling, identification and control of robots," 1st ed., Butterworth-Heinemann, pp. 291-311, 2002.

[15] M. Gautier, "Numerical calculation of the base inertial parameters," J. of Robotic Systems, Vol.8, pp. 485-506, 1991.

[16] M. Gautier and G. Venture, "Identification of standard dynamic parameters of robots with positive definite inertia matrix," IEEE/RSJ Int. Conf. on Int. Robots and Systems, pp. 5815-5820, 2013.

[17] J. Swevers, C. Ganseman, D. B. Tukel, J. de Schutter, and H. Van Brussel, "Optimal robot excitation and identification," IEEE Trans. on Robot. Autom., Vol.13, pp. 730-740, 1997.

[18] G. Calafiore, M. Indri, and B. Bona, "Robot dynamic calibration: optimal excitation trajectories and experimental parameter estimation," J. of Field Robotics, Vol.18, pp. 55-68, 2001.

[19] W. Rackl, R. Lampariello, and G. Hirzinger, "Robot excitation trajectories for dynamic parameter estimation using optimized B-Splines," IEEE Int. Conf. on Robot. Autom., pp. 2042-2047, 2012.

[20] J. Jin and N. Gans, "Parameter identification for industrial robots with a fast and robust trajectory design approach," Robotics and Computer-Integrated Manufacturing, Vol.31, pp. 21-29, 2015.

[21] S. J. Qin and T. A. Badgwell, "A survey of industrial model predictive control technology," Control Engineering Practice, Vol.11, No.7, pp. 733-764, 2003.

[22] E. F. Camacho and C. Bordons, "Model Predictive Control," Springer Science Business Media, 2013.

[23] D. W. Clarke, C. Mohtadi, and P. S. Tuffs, "Generalized predictive control – Part I. The basic algorithm," Automatica, Vol.23, No.2, pp. 137-160, 1987.

[24] D. Clarke, "Application of generalized predictive control to industrial processes," IEEE Control Systems Magazine, Vol.8, No.2, pp. 49-55, 1988.

[25] L. K. Rincon, "Study of the dynamic behavior of CNC machine tool with emphases on the implementation of control systems," Ph.D. thesis, UNICAMP, 2013.

[26] S.A. Ajwad, J. Iqbal, M. I. Ullah, and A. Mehmood, "A systematic review of current and emergent manipulator control approaches," Frontiers of Mechanical Engineering, Vol.10, No.2, pp. 198-210, 2015.

[27] J. M. Maciejowski, "Predictive Control with Constraints," Prentice Hall, 2000.

[28] M. Makarov et al, "Generalized predictive control of an anthropomorphic robot arm for trajectory tracking," 2011 IEEE/ASME Int. Conf. on Advanced Intelligent Mechatronics (AIM), 2011.

[29] A. P. Aguiar, J. P. Hespanha, and P. V. Kokotovic, "Performance limitations in reference tracking and path following for nonlinear systems," Automatica, Vol.44, No.3, pp. 598-610, 2008.

[30] K. Holkar and L. Waghmare, "An overview of model predictive control," Int. J. of Control and Automation, Vol.3, No.4, pp. 47-63, 2010.

[31] K. J. Latawiec, "Extended horizon adaptive model algorithmic control," IFAC Proc. Vol.30, No.11, pp. 305-310, 1997.

[32] A.-L. Elshafei, G. A. Dumont, and A. Elnaggar, "Adaptive GPC based on Laguerre-filters modelling," Automatica, Vol.30, No.12, pp. 1913-1920, 1994.

[33] T. Henmi, "Control Parameters Tuning Method of Nonlinear Model Predictive Controller Based on Quantitatively Analyzing," J. Robot. Mechatron., Vol.28, No.5, pp. 695-701, 2016.

[34] T. Katsumata, B. Navaro, V. Bonnet, P. Fraisse, A. Crosnier, and G. Venture, "Optimal exciting motion for fast robot identification. Application to contact painting tasks with estimated external forces," Robotics and Autonomous System (in press).

[35] D. Tolani, A. Goswami, and N. Badler, "Real-time inverse kinematics techniques for anthropomorphic limbs," Graphical Models, Vol.62, pp. 353-388, 2000.

[36] W. Khalil and D. Creusot, "SYMORO+ : A system for the symbolic modeling of robots," Cambridge J. of Robotica, Vol.15, pp. 153-161, 1997.

[37] M. Gautier and S. Briot, "New Method for Global Identification of the Joint Drive Gains of Robots using a Known Payload Mass," Proc. of the IEEE/RSJ Int. Conf. on Intelligent Robots and Systems (IROS 2011), San Francisco, CA, USA, September 25-30, 2011.

[38] W. Khalil, M. Gautier, and P. Lemoine, "Identification of the payload inertial parameters of industrial manipulators," IEEE Int. Conf. on Robot. Autom., pp. 4943-4948, 2007.

[39] T. Katsumata and G. Venture, "Adaptive Cartesian force control using payload dynamics and geometric identification," Tokyo University of Agriculture and Technology, Master thesis, pp. 43-51, 2017 (in Japanese).

[40] K. J. Park, "Fourier-based optimal excitation trajectories for the dynamic identification of robots," Cambridge J. of Robotica, Vol.24, pp. 625-633, 2006.

[41] J. de Schutter and H. V. Brussel, "Compliant robot motion II. A control approach based on external control loops," Int. J. of Robotics Research, Vol.7, pp. 18-33, 1988.

[42] A. De Luca, B. Siciliano, and L. Zollo, "PD control with on-line gravity compensation for robots with elastic joints: Theory and experiments," Automatica, Vol.41, No.10, pp. 1809-1819, 2005.

[43] J. J. E. Slotine and W. Li, "Applied nonlinear control," Prentice Hall, 1991.

[44] W. Khalil and E. Dombre, "Modeling, Identification and Control of Robots," Butterworth-Heinemann, 2004.

[45] S. Masuda, T. Yamamoto, and M. Ooshima, "Model Predictive Control-III: Generalized Predictive Control (GPC) and the Relevant Topics," Systems, Control and Information, Vol.46, No.9, pp. 578-584, 2002 (in Japanese).

[46] I. Landau, "The RST digital controller design and applications," Control Engineering Practice, Vol.6, No.2, pp. 155-165, 1998.

[47] C. Decker et al., "Application of constrained receding horizon predictive control to a benchmark problem," European J. of Control, Vol.1, No.2, pp. 157-165, 1995.

Supporting Online Materials:

[a] Toshiba, "Sensor- less compliance control for assembly robots." http://www.toshiba-machine.co.jp/en/technology/techcatalog/e3.html [Accessed January 15, 2017]

[b] M. Cefalo, "Notes on the Kuka LWR4 dynamic model." http://www.coppeliarobotics.com/contributions/LBR4p_dynamic_model.pdf [Accessed February 20, 2017]

Name:
Shohei Hagane

Affiliation:
Graduate Student, Department of Mechanical Systems Engineering, Tokyo University of Agriculture and Technology

Address:
2-24-16 Nakacho, Koganei City, Tokyo 184-8588, Japan

Brief Biographical History:
2018- Graduate Student, Tokyo University of Agriculture and Technology

Main Works:
• "Adaptive cartesian force control using payload dynamics and geometric identification," Robomech 2017, 1P1-H11, 2017.
• "Adaptive Generalized Predictive Control for 7 DoF Robot Arm," 23th Robotics Symposia, pp. 324-329, 2018.

Membership in Academic Societies:
• The Japan Society of Mechanical Engineers (JSME)

Name:
Liz Katherine Rincon Ardila

Affiliation:
Assistant Professor, Department of Mechanical Systems Engineering, Tokyo University of Agriculture and Technology

Address:
2-24-16 Nakacho, Koganei City, Tokyo 184-8588, Japan

Brief Biographical History:
2003- Project Engineer, Enterprise Advanced Automation S.A.
2008- Professor, Faculty of Engineering, Department of Electronic Engineering, Central University (Colombia)
2012- Visiting Researcher, L'Ecole Supérieure d'électricité, SUPELEC
2014- Project Coordinator/Researcher, Center of BioNanoManufacturing, Laboratory of Micromanufacturing, Institute for Technological Research of São Paulo
2016- Assistant Professor, Tokyo University of Agriculture and Technology

Main Works:
• "Study of the dynamic behavior of CNC machine tool with emphases on the implementation of control systems," Doctoral thesis, University of Campinas, T/UNICAMP R471e, February 2013.
• "Influence of Nonlinear Friction and Disturbance in the Control of a Mechatronic System: CNC Machine Tool Application," Int. Conf. Mechatronics and Embedded Systems and Applications (ASME/IEEE), Vol.3, pp. 699-706, 2011.
• "Conceptual Bases of Robot Navigation Modeling, Control and Applications," A. Barrera (Ed.), "Advances in Robot Navigation," 1ed., IntechOpen, pp. 3-28, 2011.
• "Adaptive Fuzzy and Predictive Controllers for expressive robot arm movement during human and environment interaction," Int. J. of Mechanical Engineering and Robotics Research (IJMERR), 2018.

Membership in Academic Societies:
• The Institute of Electrical and Electronics Engineers (IEEE)
• International Federation for the Promotion of Mechanism and Machine Science (IFToMM)

Name:
Takuma Katsumata

Affiliation:
Software Engineer, Yahoo Japan Corporation

Address:
Kioi Tower, Tokyo Garden Terrace Kioicho, 1-3 Kioicho, Chiyoda-ku, Tokyo 102-8282, Japan

Brief Biographical History:
2015- Graduate Student, Tokyo University of Agriculture and Technology
2017- Yahoo Japan Corporation

Main Works:
• "Adaptive cartesian force control using payload dynamics and geometric identification," Robomech 2017, 1P1-H11, 2017

Name:
Vincent Bonnet

Affiliation:
Associate Professor, Electrical Engineering and Robotics, University of Paris-Est Créteil

Address:
61 Avenue Général de Gaulle, 94000 Créteil, France

Brief Biographical History:
2009 Received Ph.D. degree in Automatics Control and Robotics from the University of Montpellier
2016- Associate Professor, Electrical Engineering and Robotics, University of Paris-Est Créteil

Main Works:
• V. Bonnet, K. Pfieffer, P. Fraisse, A. Crosnier, and G. Venture, "Self-generation of optimal exciting motions for identification of a humanoid robot," Int. J. of Humanoid Robotics, 2018.
• V. Bonnet, V. Richard, V. Camomilla, G. Venture, A. Cappozzo, and R. Dumas, "Joint kinematics estimation using a multi-body kinematics optimisation and an extended Kalman filter, and embedding a soft tissue artefact model," J. of Biomechanics, Vol.62, pp. 148-155, 2017.
• V. Bonnet, P. Fraisse, A. Crosnier, M. Gautier, and G. Venture, "Optimal Exciting Dance for Identifying Inertial Parameters of an Anthropomorphic Structure," IEEE Trans. on Robotics, Vol.32, pp. 823-836, 2016.

Name:
Philippe Fraisse

Affiliation:
Professor, Université de Montpellier

Address:
LIRMM, 161 Rue ADA, 34095 Montpellier, France

Brief Biographical History:
1988 Received Master of Electrical Engineering from Ecole Normale Supérieure de Cachan
1994 Received Ph.D. degree in Automatic Control from Université de Montpellier 2
2007- Professor, Université de Montpellier

Main Works:
• A. Cherubini, R. Passama, A. Crosnier, A. Lasnier, and P. Fraisse, "Collaborative manufacturing with physical human-robot interaction," Robotics and Computer-Integrated Manufacturing, Vol.40, pp. 1-13, 2016.
• V. Mariano Gonçalves, P. Fraisse, A. Crosnier, and B. V. Adorno, "Parsimonious Kinematic Control of Highly Redundant Robots," IEEE Robotics and Automation Letters, Vol.1, pp. 65-72, 2016.
• S. Lengagne, N. Ramdani, and P. Fraisse, "Planning and Fast Replanning Safe Motions for Humanoid Robots," IEEE Trans. on Robotics, Vol.27, No.6, pp. 1095-1106, 2011.
• P. Fraisse and A. Lelevé, "Teleoperation Over IP Network: Network Delay Regulation and Adaptive Control," Autonomous Robots, Vol.15, No.3, pp. 225-235, 2003.

Membership in Academic Societies:
• The Institute of Electrical and Electronics Engineers (IEEE)

Name:
Gentiane Venture

Affiliation:
Tokyo University of Agriculture and Technology

Address:
2-24-16 Nakacho, Koganei City, Tokyo 184-8588, Japan

Brief Biographical History:
2000- PSA-Peugeot Citroen
2004- The University of Tokyo
2009- Tokyo University of Agriculture and Technology

Main Works:
• G. Venture, P.-J. Ripert, W. Khalil, M. Gautier, and P. Bodson, "Modelling and identification of passenger car dynamics using robotics formalism," IEEE Trans. on Intelligent Transportation Systems, Vol.7, No.3, pp. 349-359, 2006.
• K. Ayusawa, G. Venture, and Y. Nakamura, "Identifiability and Identification of Inertial Parameters Using the Underactuated Base-Link Dynamics for Legged Multibody Systems," Int. J. Robotics Research, Vol.33, No.3, pp. 446-468, 2013.
• V. Bonnet, P. Fraisse, A. Crosnier, M. Gautier, A. Gonzalez, and G. Venture, "Optimal Exciting Dance for Identifying Inertial Parameters of an Anthropomorphic Structure," IEEE Trans. in Robotics, Vol.32, No.4, pp. 823-836, 2016.

Membership in Academic Societies:
• The Institute of Electrical and Electronics Engineers (IEEE)
• Japanese Society of Kansei Engineering (JSKE)
• Japanese council of the International Federation for the Promotion of Mechanism and Machine Science (Jc-IFToMM)